AMB2022-03 Benchmark Measurements and Challenge Problems

Last updated on 5/26/2022

Modelers are invited to submit simulation results for any number of challenges they like before the deadline of 23:59 (ET) on July 15, 2022. Tabulated results using the challenge-specific templates are required for most challenge problems and simulation results may be submitted **here**. An informational webinar for AMB2022-03 will be held on May 5, 2022, from 13:15 – 14:15 Eastern Time. The webinar registration link is **here**. After the webinar is completed, links to the recorded presentations and to a FAQ page will be added to the AMB2022-03 description page. Additional information may become available later so updated versions of this document may be posted. Please check back occasionally.

All evaluations of submitted modeling results will be conducted by the AM-Bench 2022 organizing committee. Award plaques will be awarded at the discretion of the organizing committee. Because some participants may not be able to share proprietary details of the modeling approaches used, we are not requiring such details. However, whenever possible we strongly encourage participants to include with their submissions a .pdf document describing the modeling approaches, physical parameters, and assumptions used for the submitted simulations.

Please note that the challenge problems reflect only a small part of the validation measurement data provided by AM Bench for each set of benchmarks. The Measurement Descriptions section, below, describes the full range of measurements conducted.

AMB2022-03: Single laser tracks using different processing conditions and 2D arrays of laser tracks (Pads) on solid plates of IN718. Detailed descriptions are found below, and simulation results may be submitted **here**.

Challenges

- Track Solid Cooling Rate (CHAL-AMB2022-03-TSCR): Cooling rate immediately following complete solidification (below solidus) at the center of each track for all processing conditions.
- Track Liquid Cooling Rate (CHAL-AMB2022-03-TLCR): Liquid cooling rate immediately before start of solidification (above liquidus) at the center of each track for all processing conditions.
- Track Time Above Melt (CHAL-AMB2022-03-TTAM): Time above the midpoint between solidus and liquidus temperature (assumed to be 1 298 °C) for single laser-scanned tracks.
- Track Melt Pool Geometry (CHAL-AMB2022-03-TMPG): The laser track width and depth near the center of each track for all processing conditions.
- Pad Solid Cooling Rate (CHAL-AMB2022-03-PSCR): Cooling rate immediately following complete solidification (below solidus) at the center of each track for all processing conditions.
- Pad Time Above Melting (CHAL-AMB2022-03-PTAM): Time above the midpoint between solidus and liquidus temperature (assumed to be 1 298 °C) for specified locations of the X-Pads and Y-Pads.

- Pad Melt Pool Geometry (CHAL-AMB2022-03-PMPG): Laser track depth and geometrical measurements describing the overlapping laser tracks near the center and near the edge of both X-Pads and Y-Pads.

Document Updates from original release Version 1.00

Version 1.01 – Created on 5/26/2022

- Errors in the CHAL-AMB2022-03-PMPG and CHAL-AMB2022-03-TMPG submission templates have been corrected. Links now point to these updated templates.

---

1. Overview and Basic Objectives

The AMB2022-03 benchmarks explore a range of individual and overlapping melt pool behaviors using individual laser tracks and 2D arrays of laser tracks on solid metal IN718 plates. For the individual laser tracks, a range of laser parameters were used, with variations in laser power, speed, and spot diameter. In situ measurements include time-resolved laser coupling, location-specific liquid and solid cooling rates, and location specific time above melting. Ex situ measurements include 3D topography of the solidified laser tracks and cross-sectional geometry and microstructure measurements. For the 2D pads, scan patterns and timing match those used for the odd (X-Pads) and even layers (Y-Pads) of the AMB2022-01 3D builds. The same sets of in situ and ex situ measurements used for the single laser tracks were used for the laser pad studies.

2. Sample and Laser Processing

2.1 Plate preparation:

Sample substrates were cut from a rolled and annealed IN718 sheet (given MaterialID AMB2022-718-SH1, see Section 2.5). Material certificate for the as-received IN718 sheet is available **here**.

The following steps were taken to prepare the samples:

- 3.17 mm (1/8”) thick IN718 sheet was cut to produce 25.4 mm x 25.4 mm (1” x 1”) bare plates
- The bare plates were random-orientation polished with 320 grit SiC paper
- The bare plates were residual stress annealed in vacuum at 800 °C for 2 h. This anneal was in preparation for possible future synchrotron X-ray measurements of elastic strains produced by the laser tracks.
- The bare plates were random-orientation polished again with 320 grit SiC paper. The typical resulting surface roughness was Ra = 5.8 µm.

2.2 Laser processing parameters

All individual laser tracks and laser pads were produced using the NIST Additive Manufacturing Metrology Test Bed (AMMT) which is a NIST-designed and built laser-processing metrology platform. Detailed references to the AMMT design, controller, and various other research may be found **here**. The AMMT is also a fully functional laser powder bed fusion (LPBF) AM machine, with a continuous-wave (CW) ytterbium fiber (Yb:fiber) laser, with a central wavelength of 1070 nm, directed by fully-controllable scanning galvanometer mirrors. The controlled laser scanning is synchronized to various measurement instrument triggering and data acquisition.

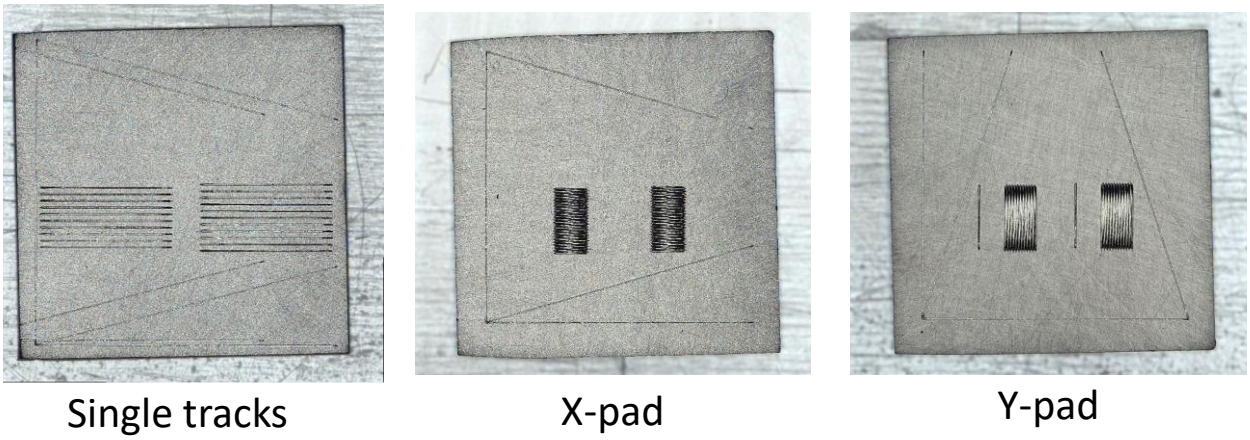

Figure 1: Example of bare plate samples with different laser scan patterns and orientations. Laser-scanned traces can also be seen which are used to align and orient samples after cutting.

Figure 1 shows examples of bare plate samples with different laser scan patterns and orientations. Samples were mounted 6 at a time within the AMMT on a custom holder shown in Figure 2. Unlike the 2018 AM-Bench samples, which were held by pins with minimal contact (e.g., thermal conduction paths), the 2022 AMMT samples are directly mounted with full contact on the bottom to a stainless steel 304 (thermal conductivity and specific heat within 30 % of IN718) baseplate and held down by two flat head screws. Each sample also had a k-type thermocouple which contacts the center underside.

A time period of at least one minute passed between the laser scanning of each track or pad to reduce effects of residual heat buildup. Thermocouples integrated with the mounting plate contacting the backside of the samples are shown in Figure 2, and all tracks were scanned at a sample temperature of 23.5 ± 1.0 °C. The temperature measured on the backside of the sample rose a total of < 0.7 °C for each pad scan, and the temperature rose < 0.1 °C after each line scan.

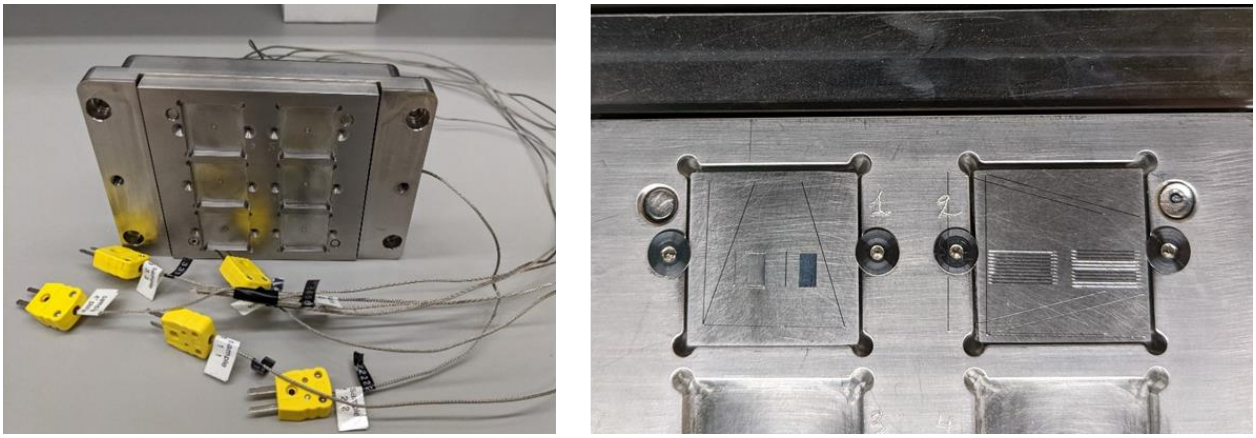

Figure 2: Left: Sample mounting cutouts within the AMMT standard build plate, including thermocouples. Right: Example of samples mounted within the AMMT holder, including a Y-pad and single-line tests.

2.2.1 Single laser track measurements with thermography

The baseline parameters are listed in Table 1, and the offset laser parameters for all seven parameter sets are listed in Table 2. Figure 3 shows the layout and numbering of single tracks on the substrates.

Table 1: AMMT laser processing conditions for single tracks scanned on bare IN718 substrates

Base laser processing conditions	
Laser power	285 W
Laser speed	960 mm/s
Pad hatch spacing	110 µm
Laser spot size (gaussian)	67 µm
Laser energy distribution	Rotationally-symmetric Gaussian
Single track scan direction	+X
Single track length	10 mm
Inert gas	Argon
Max. Oxygen level	< 1 000 ppm
Gas flow speed (Z = 10 mm)	4.3 m/s
Gas flow direction	-Y
Chamber pressure	95 ± 5 kPa
Substrate and chamber temperature	23.5 ± 1 °C
Laser incidence angle	5 ± 0.5 °
Surface roughness (R_a)	5.8 µm

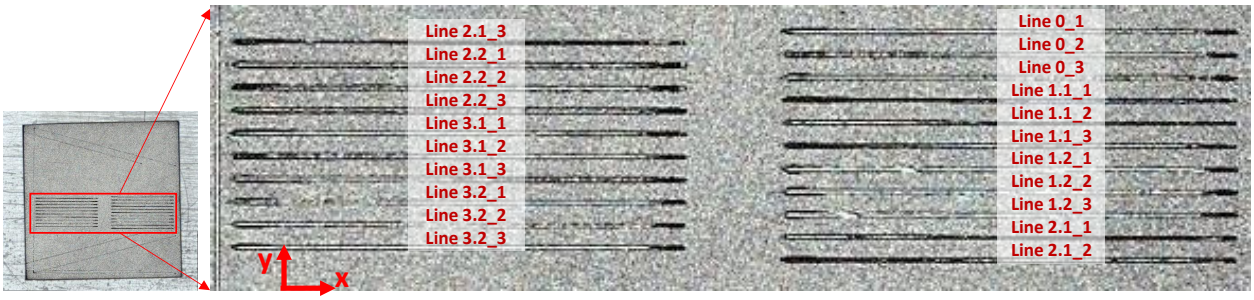

Figure 3: Layout and numbering of the 21 tracks, consisting of 7 laser scanning parameter sets (or 'case number') and 3 repeats per parameter set.

Table 2: Offset laser parameters for AMB2022-03 individual laser track thermography measurements with varying laser power, spot size, and scan speed. Each case is repeated three times for a total of 21 laser scan tracks. Volumetric energy density based on 1σ laser beam size, VEDσ, is also provided.

	Case Number	Laser Power [W]	Scan Speed [mm/s]	Spot size, D4σ [µm]	VEDσ = P/v/σ² [J/mm³]	VED/VED$_{base}$
Baseline	0	285	960	67	1058	1.00
Change spot	1.1	285	960	49	1978	1.87
	1.2	285	960	82	706	0.67
Change Speed	2.1	285	1200	67	847	0.80
	2.2	285	800	67	1270	1.20
Change Power	3.1	325	960	67	1207	1.14
	3.2	245	960	67	910	0.86

2.2.2 Laser pad measurements with thermography

The laser parameters used for the laser pad measurements are the same as those used as the baseline parameter set for the single laser track measurements described above (see Table 1 and Table 2). The scan patterns and speed match those used for the odd and even layers of the 2.5 mm thick legs of the AMB2022-01 bridge specimen. In other words, Y-Pad here matches the Y scan pattern for the odd layers of the 3D builds, and the X-Pad here matches the X scan pattern for the even layers. However, note that the spot size here is different from the 77 µm D4σ spot size used in the AMB2022-01 builds. The X-pad scans, shown in Figure 4, are the same as the 2.5 × 5 mm Leg 9 within the camera field of view. The scan order and timing are based on layer 26 from AMB2022-01 3D builds.

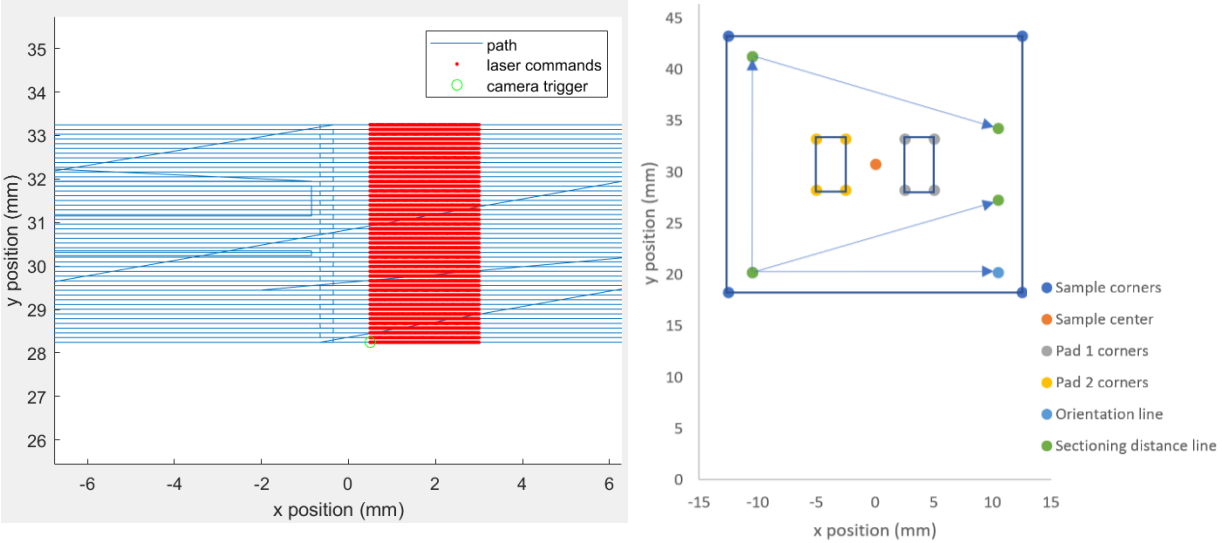

Figure 4: Left: Laser scan position. Red indicates laser is 'on', blue indicates laser is 'off'. Right: Layout geometry of the two X-pads and alignment marks.

The Y-pad scans, shown in Figure 5, are the same as the 2.5 x 5 mm Leg 9 from the AMB2022-01 bridge structure (albeit with different laser spot size) within the camera field of view, and one additional line from the 5 x 5 mm Leg 10. The scan order and timing are based on layer 27 from the AMB2022-01 3D builds.

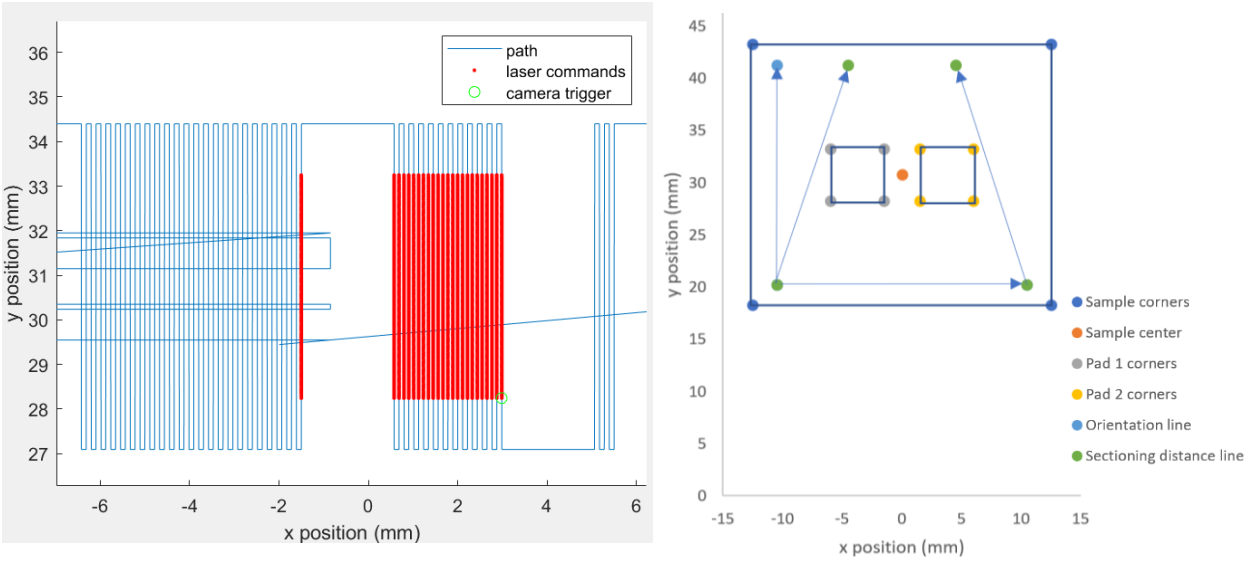

Figure 5: Left: Laser scan position. Red indicates laser is 'on', blue indicates laser is 'off'. Right: Layout geometry of the two Y-pads and alignment marks.

2.2.3 Single laser track measurements with dynamic coupling

The baseline parameters are listed in Table 3, and the offset laser parameters for all seven parameter sets are listed in Table 4. Note that the laser spot size is different from 3D builds and single laser track and pad scans with thermography measurements.

Table 3: AMMT laser processing conditions used for AMB2022-03 dynamic laser coupling measurements while scanning single tracks on IN718 bare metal substrates

Base laser processing conditions	
Laser power	285 W
Laser speed	960 mm/s
Pad hatch spacing	110 µm
Laser spot size (gaussian)	110 µm
Laser energy distribution	Rotationally-symmetric Gaussian
Single track scan direction	+Y
Single track length	10 mm
Inert gas	Argon
Max. Oxygen level	< 1 000 ppm
Gas flow speed (Z = 3 mm)	2.3 m/s
Gas flow direction	+X
Chamber pressure	101 ± 2 kPa
Substrate and chamber temperature	23.5 ± 1 °C
Laser incidence angle	8 ± 0.5 °
Surface roughness (R_a)	5.8 µm

Table 4: Offset laser parameters for AMB2022-03 individual laser track dynamic coupling measurements with varying laser power, spot size, and scan speed. Each case is repeated three times for a total of 21 laser scan tracks. Volumetric energy density based on 1σ laser beam size, VEDσ, is also provided.

	Case Number	**Laser Power [W]**	**Scan Speed [mm/s]**	**Spot size, D4σ [µm]**	**VEDσ = P/v/σ² [J/mm³]**	**VED/VED$_{base}$**
Baseline	0	285	960	110	393	1.00
Change spot	1.1	285	960	76	822	2.09
	1.2	285	960	131	277	0.71
Change Speed	2.1	285	1200	110	314	0.80
	2.2	285	800	110	471	1.20
Change Power	3.1	325	960	110	448	1.14
	3.2	245	960	110	337	0.86

2.2.4 Laser pad measurements with dynamic coupling

The laser parameters used for the pad dynamic coupling measurements are the same as those used as the baseline parameter set for the single laser track measurements described above (see Table 3 and Table 4). The scan patterns match those used for the odd and even layers of the 2.5 mm thick legs of the AMB2022-01 bridge specimen. Thus, the Y-Pad matches the Y scan pattern for the odd layers.

The Y-pad scans are the same as those used for the 2.5 x 5 mm Leg 9, but excludes the additional line shown in Figure 5. The scan order and timing are based on layer 27 from the AMB2022-01 3D builds.

2.3 Gas flow system

Inert gas flow across the laser melting process is used to remove process byproducts (metal vapor, condensate, and ejecta) from the laser path, build area, and chamber windows. Previous studies have shown that ineffective gas flow interferes with laser delivery and may result in powder bed contamination (Ladewig et al. 2016, Deisenroth et al. 2021). The AMMT gas flow system incorporates a two inlet and one outlet system, as shown in Figure 6a. As shown by the orientation of the fabric tufts in Figure 6a, the inlet locations at the top and bottom of the process enclosure prevent the formation of a recirculation zone that would reduce the efficacy of byproduct transfer to the outlet.

The total flow rate of argon through the build chamber was approximately 390 L/min. This flow rate and nozzle configuration results in spatial distributions of the gas flow speed in the Y and Z directions, which are approximately invariant in the X direction across the build area. The combined speed resulting from the Y and Z velocity components of the flow was measured by hot wire anemometry at several Y and Z locations at approximately X = 0 mm to characterize the flow across the build space. Details of the speed measurements are described in Weaver et al. 2021. As shown in Figure 6b, the gas speed at the single track and pad location (near X = 0 mm, Y = 30 mm) at Z = 10 mm is approximately 4.3 m/s, which is used as a representative gas flow speed value.

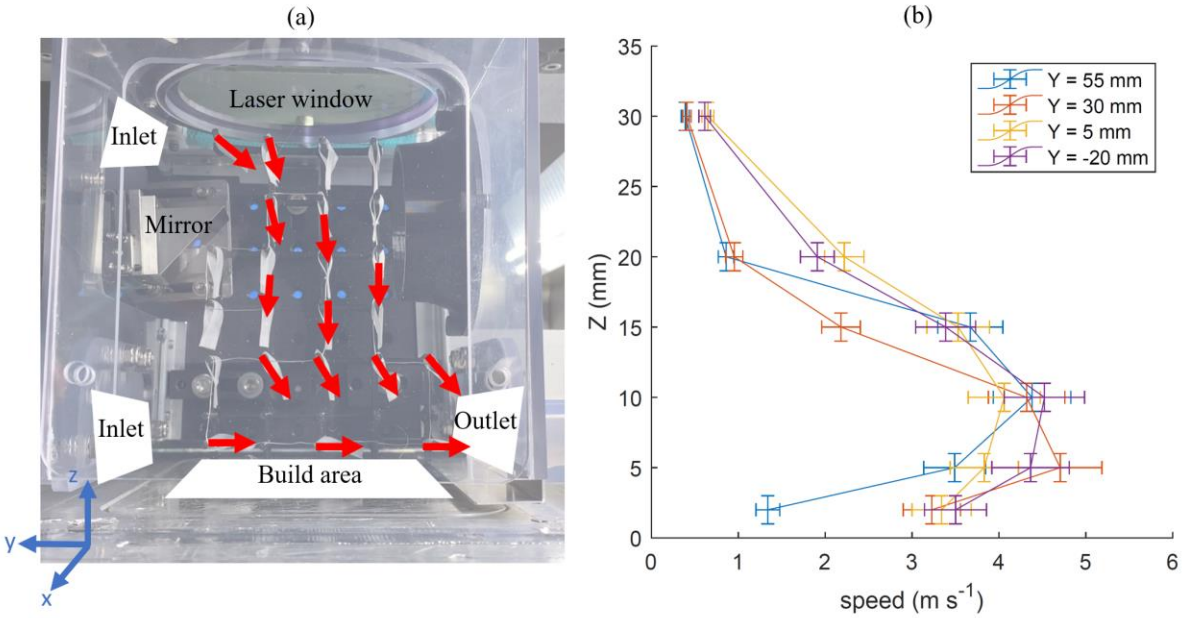

Figure 6: (a) AMMT process enclosure gas flow direction distribution based on fabric tufts. The image is flipped horizontally for ease of visualization and approximate axis directions (not origin) are shown. (b) gas flow speed distributions at varying Y and Z positions at approximately X = 0 mm.

2.4 In Situ Monitoring Systems Half of the bare plate samples were laser processed with simultaneous high-speed in situ thermography, and half were processed using in situ laser coupling measurement. The thermography samples were later cross-sectioned for optical microscopy and SEM while the laser coupling samples were measured using laser confocal microscopy.

2.4.1 Thermography: Figure 7a shows a diagram of the staring imaging system used for in situ thermographic measurements and Figure 7b shows a photograph of the completed system. To the greatest extent possible, this system was designed to provide nearly identical layer scan

patterns, measurement methods, instruments, and gas flow conditions for the sets of 3D build benchmarks (AMB2022-01 and AMB2022-02) and the 2D laser pad benchmarks (AMB2022-03).

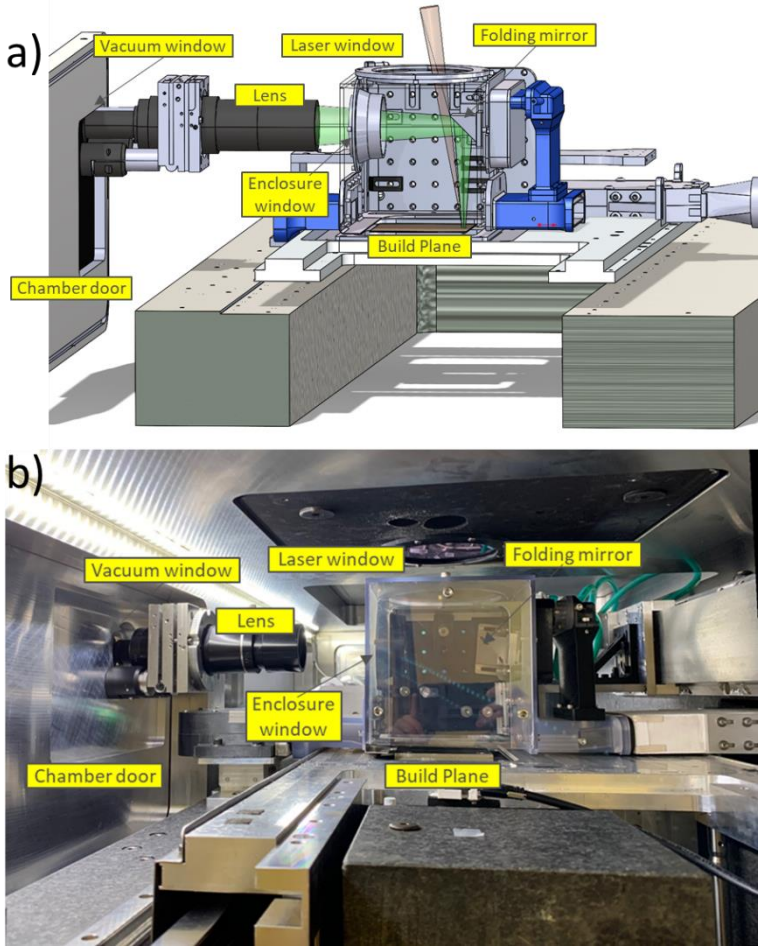

Figure 7: Staring imaging system used for in situ thermography on the AMMT, a) CAD model and b) photograph.

The properties of the camera used for the in-situ thermography measurements are given in Table 5.

Table 5: Camera properties for high-speed staring thermography camera in the AMMT

Sensor Type:	Si-based CMOS
View Angle:	~82°
Wavelengths:	830 nm to 870 nm
Magnification	1×
Window Size (x by y):	(640 by 304) pixels
iFoV (x by y)	(20.4 by 20.8) µm/pixel
FoV (x by y)	13.1 x 6.4 mm
Frame Rate	Up to 30 000 frames/s
Integration Time	20 µs
Bit depth:	12-bit (4096 DL)
Calibrated Temperature Range:	1001 °C to 1389 °C

2.5 Specimen Naming Convention

The AMB2022-03 bare plates use the following naming convention:

AMB2022-718-SH1: MaterialID for the IN718 sheet used to make square laser targets

AMB2022-718-SH1-BP1: Bare plate #1, 3 x 7 single laser tracks, in situ thermography

AMB2022-718-SH1-BP2: Bare plate #2, 2 x 2.5 mm X-axis pads, in situ thermography

AMB2022-718-SH1-BP3: Bare plate #3, 2 x 2.5 mm Y-axis pads, in situ thermography

AMB2022-718-SH1-BP4: Bare plate #4, 3 x 7 single laser tracks, in situ dynamic laser coupling

AMB2022-718-SH1-BP5: Bare plate #5, 2 x 2.5 mm X-axis pads, in situ dynamic laser coupling

AMB2022-718-SH1-BP6: Bare plate #6, 2 x 2.5 mm Y-axis pads, in situ dynamic laser coupling.

After completion of the laser scans, the in situ thermography specimens were cross-sectioned as shown in Figure 8. The naming convention for the individual cut sections is also shown in this figure.

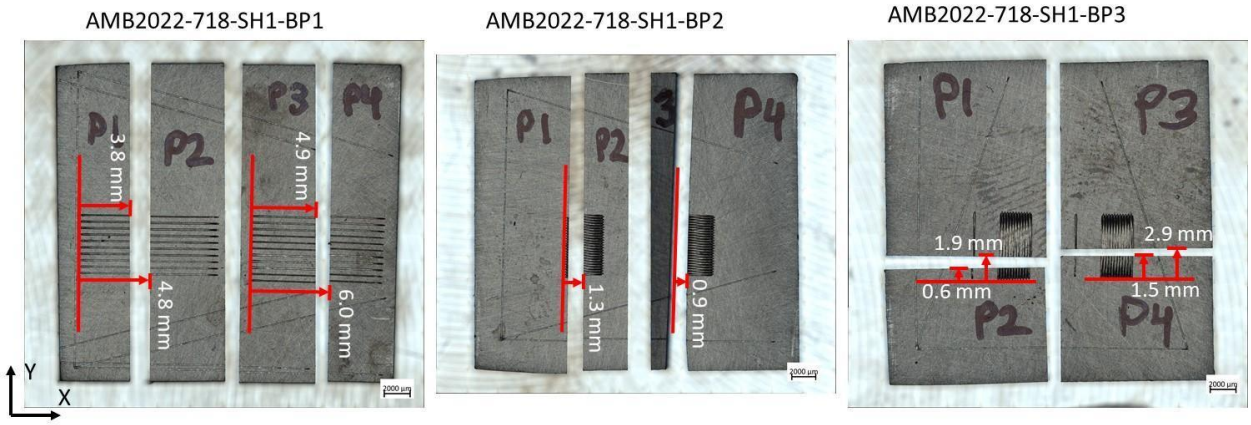

Figure 8: Bare plate sample sectioning and naming convention. The positions of cross-sections listed on each part were determined after metallographic sample preparation using fiducial markings. Red arrows are shown for schematic purposes only and do not indicate measurements from these images.

3. Measurement Descriptions

The AMB2022-03 single track and pad benchmark measurements include in situ phenomena during the laser track and pad processing and ex situ characterization of the 3D surface topography and the laser track and pad cross-sectional geometry and microstructure. The measurement methods include:

In situ measurements during laser melting

- In situ thermography to measure the location-dependent cooling rates of the melt pool immediately preceding solidification (before the liquidus is reached) and the solid material immediately after solidification (after the solidus is reached)

- In situ thermography to determine the time above melting (above the midpoint between the liquidus and solidus)
- In situ dynamic laser coupling (i.e., absorption)

Ex situ measurements

- 2D cross-sections of the thermography specimens were measured using a combination of SEM and optical microscopy
- Laser confocal microscopy was used to measure the 3D surface topography of the laser coupling specimens

3.1 In Situ Time Above Melting

Before interpreting thermographic data products, it must be noted that the metal AM process creates a challenging environment for thermography. The challenges generated by rapid melting of metals can include image attenuation and distortion, changes in the optical path distance, extraneous light sources, and more. Therefore, all model comparisons will be made to the *apparent* temperature distribution, including any and all measurement error induced by the laser-matter interaction. The measurement results used for comparison will be the average of three experimental repeats for each combination, or 'case' listed in Table 1.

The temperature history of the pixels of the thermographic images were evaluated with a comparable approach to AM-Bench 2018. The temperature history of 30 adjacent pixels along the centerline of the melt path were evaluated and aligned by the rising edges. The thermal histories were then mildly smoothed and then averaged to produce a representative thermal history of the melt pool at steady state, which is illustrated in Figure 9.

The temperature discontinuity that indicates solidification was identified and fit with a cubic polynomial curve in a range of approximately ±50 °C of the apparent inflection point. The location at which the second derivative of the curve fit reached zero was then identified as the inflection point. The time between the corresponding inflection temperature at front and rear of the melt pool is the time above melting (TAM).

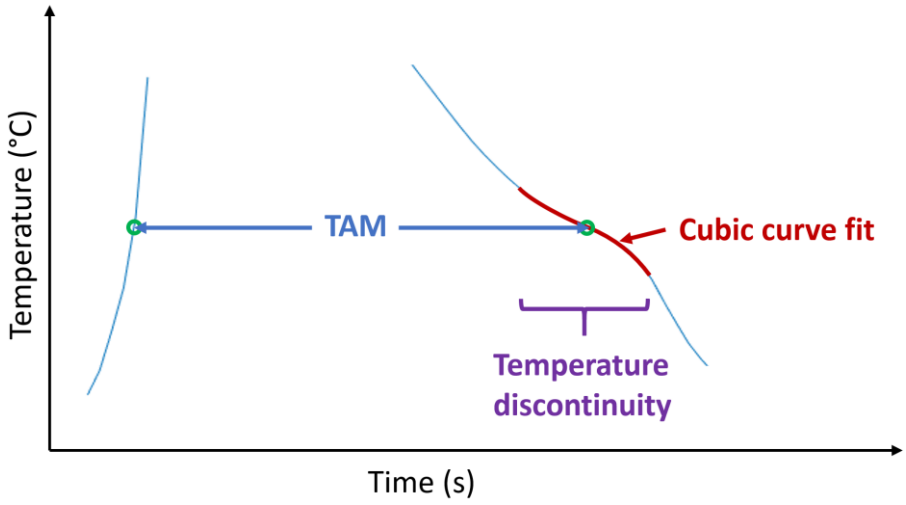

Figure 9: Illustration of a representative steady-state centerline melt pool temperature history, the temperature discontinuity at solidification, and measurement of the TAM.

3.2 In Situ Cooling Rates

The established inflection point is assumed to be the midpoint between the nominal solidus and liquidus temperatures of 1 260 °C and 1 336 °C, respectively. As illustrated in Figure 10, three distinct cooling rates (CRs) can be identified from this approach. The CRs are found by the slope of a linear fit of the temperature data between two reference temperatures: the liquid CR is taken from 1 400 °C to the liquidus, the transition CR is taken from the liquidus to the solidus, and the solid CR is taken from the solidus to 1 150 °C.

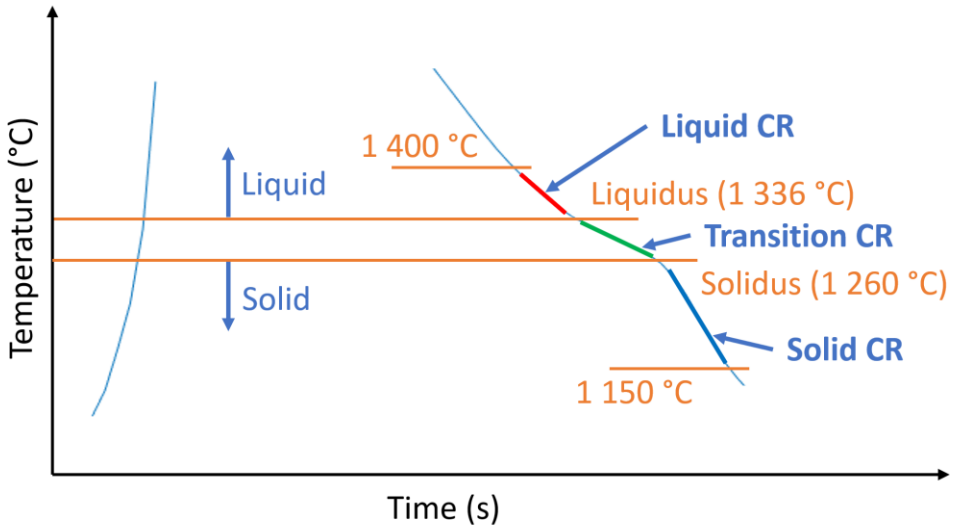

Figure 10: Illustration of the temperature ranges and linear fits used to establish three distinct CRs.

3.3 In-situ Dynamic Laser Coupling

Additional measurements were performed on the AMMT to acquire dynamic laser energy coupling (i.e., time-resolved reflected laser power) using a reflectometer-based method described in Deisenroth et al. 2020, and producing similar results to the 2022 Asynchronous AM-Benchmark tests (A-AMBench2022). This method utilizes a hemispherical reflectometer, which is calibrated to measure the time-varying amount of laser power reflected from the laser processing area. These measurements were acquired for the same laser processing parameters (except for a different laser diameter) as the single tracks and vertical and horizontal pads measured via high-speed thermography as described in Section 2.2. No challenge problems will be associated with these measurements; however, the results and data will be released in July 2022 for model comparisons.

3.4 2D Cross Sections

Cross-sections were made perpendicular (within 2° perpendicular) to laser tracks and pads using a rubber bond alumina abrasive blade (0.762 mm thickness) on a high-speed precision saw. Samples

were metallographically prepared and etched with Aqua Regia. Micrographs of the melt-pools were taken with optical microscopy using bright field and dark field imaging.

Cross-section locations were determined from fiducial laser tracks. The fiducial laser tracks were measured on the top surface prior to cross-sectioning and on the side surface of metallographically prepared cross-sections. The cross-section locations are relative to the left side of single tracks and X-pads and the bottom side of Y-pads as shown in Figure 8.

3.4.1 Optical microscopy

Melt-pool depth and width measurements were made on optical micrographs. These are schematically shown in Figure 11. Because there is no powder in these experiments, the melt-pool depths are defined from the plate's top surface ignoring any humping of material above the starting surface. Depth measurements are perpendicular to the top surface and width measurements are parallel to the top surface. The depths, d_t and d_p, are always the largest distance, not necessarily in the center of the melt-pool. The pad overlap depth, d_o, is the greatest distance from the top surface to where melt pools intersect. The widths are always the widest distance, not necessarily at the top surface. The pad width, w_p, is measured from the depth line, d_p, to the widest point of the melt pool. The pad overlap width, w_o, is the distance between the widest point of a melt pool and its succeeding melt pool (e.g., w_{o_1} is measured between track 1 and track 2). These points need not be in the same Z-plane.

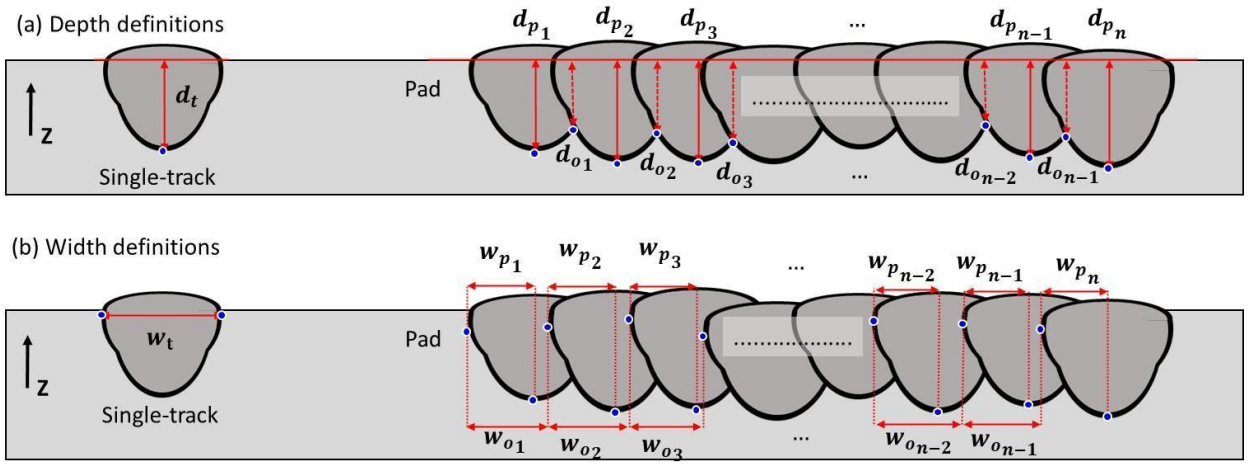

Figure 11: Schematic definitions of melt pool cross-section measurements for single tracks and pads. Blue dots indicate measurement points. Pad scans start at track 1 and end at track 'n'. Melt-pool shapes may vary based on process variables, and the schematic is nothing more than a simple illustration.

3.4.2 Scanning electron microscopy

Cross-sections were prepared by progressive polishing from 600 grit SiC paper down to 1 µm diamond suspension. Final surface preparation used vibro-polishing with 0.05 µm non-colloidal silica for 16 h. Samples were cleaned in an ultrasonic bath in three solutions: soap/water, water, and ethanol.

Imaging and data acquisition were performed using a JEOL Field Emission JSM7100† with the Oxford Symmetry S2 EBSD detector† with fore-scatter diodes and the Oxford Ultim Max EDS 100 mm2 silicon

drift detector. Oxford Aztec† software Ver 6.0 was used for EDS/EBSD analysis and to create large area maps. The SEM measurement conditions are listed in Table 6.

Table 6: SEM settings used for the 2D cross-section measurements

SEM settings	20 kV	10 nA	70 deg tilt	Working distance ~ 25 mm	400 x magnification Field of view = 300 pixels x 226 pixels (0.3 mm x 0.23 mm)
EBSD settings	Rectangular, Cover Area	1 um step	20 % overlap	Acq. speed = 2 Speed 2 Resolution = (156 pixels x 128 pixels) Exposure time ~ 6 ms	Saved EBSD patterns

3.3.3 Laser scanning confocal microscopy

As described above, multiple single laser tracks and 2D pads of laser tracks were produced on bare metal plates of IN718 while measuring the dynamic laser coupling in situ. These plates, AMB2022-718-SH1-BP4 (single laser tracks), AMB2022-718-SH1-BP5 (X-pads), and AMB2022-718-SH1-BP6 (Y-pads), were measured ex situ using laser scanning confocal microscopy. The complete 3D surface profiles of the laser tracks and pads were measured to extract information on the height profiles under steady state conditions, the mass accumulations and losses at the ends of the tracks, the shapes of the chevron features, and the effect of multiple adjacent tracks on the height profiles. No challenge problems will be associated with these measurements; however, the results and data will be released in July 2022 for model comparisons.

4. Description of Benchmark Challenge Problems

4.1 Single Laser Track Benchmarks

4.1.1 CHAL-AMB2022-03-TTAM

Modelers are to calculate the single track ‘time above melting’ as close as possible to the definition described in Section 3.1 for all seven combinations of laser power, scan speed, and spot size listed in Table 2. Modelers should provide a TAM during steady state for each of the of the seven parameter

combinations rounded to three significant digits, in units of seconds. Modelers will be judged by calculating the RMS error between the modeled and measured values, as follows:

$$\Delta_{TAM} = \sqrt{\sum_{i=1}^{7}(TAM_i - TAM_{i,model})}^{2}$$

A template for submissions is provided **here**. Note that TTAM, TSCR, and TLCR challenges are included in the same template, but are considered separate challenges.

4.1.2 CHAL-AMB2022-03-TSCR

Modelers are to calculate the single track 'solid cooling rate' as close as possible to the definition described in Section 3.2 for all seven combinations of laser power, scan speed, and spot size listed in Table 2. Modelers should provide a SCR for each of the of the seven parameter combinations rounded to three significant digits in units of °C/s. Modelers will be judged by calculating the RMS error between the modeled and measured values, as follows:

$$\Delta_{SCR} = \sqrt{\sum_{i=1}^{7}(SCR_i - SCR_{i,model})}^{2}$$

The measurement, judging, and model comparison notes described in the TTAM section, above, also apply to the TSCR competition. A template for submissions is provided **here**. Note that TTAM, TSCR, and TLCR challenges are included in the same template, but are considered separate challenges.

4.1.3 CHAL-AMB2022-03-TLCR

Modelers are to calculate the single track 'liquid cooling rate' as close as possible to the definition described in Section 3.2 for all seven combinations of laser power, scan speed, and spot size listed in Table 2. Modelers should provide a LCR for each of the of the seven parameter combinations rounded to three significant digits. Modelers will be judged by calculating the RMS error between the modeled and measured values, as follows:

$$\Delta_{LCR} = \sqrt{\sum_{i=1}^{7}(LCR_i - LCR_{i,model})}^{2}$$

The measurement, judging, and model comparison notes described in the TTAM section, above, also apply to the TLCR competition. A template for submissions is provided **here**. Note that TTAM, TSCR, and TLCR challenges are included in the same template, but are considered separate challenges.

4.1.4 CHAL-AMB2022-03-TMPG

The measurement average and standard deviation for each case number are determined from three repeat tracks and four cross-sections (P1, P2, P3, and P4). Predict the average melt pool depth and width for the seven case numbers at the midpoint along the track length in micrometers. Modelers will be judged by calculating the RMS error between the modeled and measured values, as follows:

$$\Delta_{TMPG} = \sqrt{\sum_{i=1}^{7}\left(d_{t_i} - d_{t_{i,model}}\right)^2} + \sqrt{\sum_{i=1}^{7}\left(w_{t_i} - w_{t_{i,model}}\right)^2}$$

A template for submissions is provided **here**. Please note that this template is updated from the original version.

4.2 Laser Pad Benchmarks

4.2.1 CHAL-AMB2022-03-PTAM

Modelers are to calculate 'time above melting' as close as possible to the definition or algorithm described in the 3D build CHAL-AMB2022-01-TAM. Modelers should calculate TaM values within the X-pads and Y-pads (described in Figure 4 and Figure 5), excluding the additional line adjacent to the Y-pad. Modelers should then calculate the following statistical features for the CHAL-AMB2022-03-PTAM modelling challenge:

- Number of pixel/element/nodes that TaM is interrogated from model results (e.g., sample size)
- Mean of all pixel/element/nodal TaM values
- Median of all pixel/element/nodal TaM values
- Standard deviation of all pixel/element/nodal TaM values

The measurement, judging, and model comparison notes described in the TTAM section, above, also apply to the PTAM competition. Additionally, modelers should supply pictures and/or a brief description of the model formulation (e.g., finite element, finite difference, boundary element, etc.) and visualizations of results. These will be used by AM-Bench organizers to select and request submission of invited papers to a special journal issue.

Note that it is not expected that the AM simulation outputs exactly replicate the temporal, spatial, or temperature resolution or range of the thermographic imaging system, and model formulations may utilize certain approximations that render results outputs that are less-physically equivalent to the thermographic measurements described in Section 3.1. Therefore, participants should consider the following:

1) In calculating the above statistical features, modelers should reject values outside the measurable/calculable TaM results (e.g., reject '0' values). Modelers may also wish to reject statistical outliers.
2) Depending on the model formulations, modelers may also consider testing or utilizing different algorithms or definitions of 'time above melt' (e.g., using a different threshold temperature). However, for the modeling challenge, model results will be compared against measurement results as described in Section 3.1. Only one entry from each participating research group will be used for the challenge judging.

A template for submission is provided **here**.

4.2.2 CHAL-AMB2022-03-PSCR

Modelers should calculate SCR values as close as possible to the definition or algorithm described in the 3D build CHAL-AMB2022-01-SCR. Modelers should calculate SCR values within the X-pads and Y-pads (described in Figure 4 and Figure 5), excluding the additional line adjacent to the Y-pad. Modelers should then calculate the following statistical features for the CHAL-AMB2022-03-PSCR modeling challenge:

- Number of pixel/element/nodes that SCR is interrogated from model results (e.g., sample size)
- Mean of all pixel/element/nodal SCR values
- Median of all pixel/element/nodal SCR values
- Standard deviation of all pixel/element/nodal SCR values

The measurement, judging, and model comparison notes described in the TTAM and PTAM sections above also apply to the PSCR competition.

4.2.3 CHAL-AMB2022-03-PMPG

The measurement average and standard deviation are determined for odd and even track numbers on cross-sections (e.g., AMB-2022-718-SH1-BP2-P2-Odd, AMB-2022-718-SH1-BP2-P2-Even). For BP2, Odd numbered tracks scan in the +X direction and even numbered tracks scan in the -X direction. For BP3, Odd numbered tracks scan +Y direction and even numbered tracks scan in the -Y direction. Note the pad starting points are indicated in Figure 4 and Figure 5 by the green circles. Predict the average melt pool depths and widths as described in Section 3.3 for odd and even track numbers for each cross-section in micrometers (two cross-sections for BP2 and four cross-sections for BP3). Cross-section positions are given in Figure 11. Modelers will be judged by calculating the RMS error between the modeled and measured values, as follows:

$$\Delta_{PMPG} = \sqrt{\sum_{i=1}^{4}\left(\left(x_i - x_{i,model}\right)^2{}_{Odd} + \left(x_i - x_{i,model}\right)^2{}_{Even}\right)},$$
$$x_1 = d_p, x_2 = d_o, x_3 = w_p, x_4 = w_o.$$

A template for submissions is provided **here**. Please note that this template is updated from the original version.

5. Description and Links to Associated Data

All data available to support the AMB2022-03 challenges are linked directly within this document. Updates and/or changes to download URLs may be made periodically. Users should refer to the top of this document or webpage for updates.

6. References

Citations are provided throughout this document as hyperlinked URLs to the associated digital object identifier (DOI). Clicking these hyperlinked text should open the associated publication or cited source.

†Disclaimer

The National Institute of Standards and Technology (NIST) uses its best efforts to deliver high-quality copies of the AM Bench database and to verify that the data contained therein have been selected on the basis of sound scientific judgment. However, NIST makes no warranties to that effect, and NIST shall not be liable for any damage that may result from errors or omissions in the AM Bench databases.

Certain commercial equipment, instruments, or materials are identified in this paper in order to specify the experimental procedure adequately. Such identification is not intended to imply recommendation or endorsement by NIST, nor is it intended to imply that the materials or equipment identified are necessarily the best available for the purpose.